Improved ordered subsets algorithm for 3D X-ray CT image reconstruction

Donghwan Kim, Debashish Pal, Jean-Baptiste Thibault, and Jeffrey A. Fessler

***Abstract*—Statistical image reconstruction methods improve image quality in X-ray CT, but long compute times are a drawback. Ordered subsets (OS) algorithms can accelerate convergence in the early iterations (by a factor of about the number of subsets) provided suitable "subset balance" conditions hold. OS algorithms are most effective when a properly scaled gradient of each subset data-fit term can approximate the gradient of the full data-fidelity term. Unfortunately, this property can fail in the slices outside a region-of-interest (ROI) of 3D CT geometries where sampling becomes limited, particularly for large numbers of subsets, leading to undesirable results. This paper describes a new approach to scaling the subset gradient for a regularized OS algorithm so that it better approximates the full gradient outside the ROI. We demonstrate that the new scaling factors improve stability and image quality in helical CT geometry, even for a very large number of subsets.**

I. Introduction

Statistical image reconstruction methods can improve resolution and reduce noise and artifacts by minimizing a cost function that models the physics and statistics in X-ray CT [1]. The primary drawback of these methods is their computationally expensive iterative algorithms. Ordered subsets (OS) algorithms group the projection data into (ordered) subsets and update the image each sub-iteration using one forward and back projection of just one subset [2], [3]. OS methods can accelerate convergence (by a factor of about L, the number of subsets) in the early iterations, so it is desirable to use many subsets[1]. OS methods are most effective when suitable "subset balance" conditions hold. Unfortunately, the "long object problem" in CT hampers subset balance, particularly for large L. This paper describes a new approach that improves OS methods for helical CT with large L (many subsets).

In CT, the user defines a target region-of-interest (ROI) for reconstruction. Iterative reconstruction algorithms must estimate more voxels than the ROI to model the measured data completely. In particular, in helical CT, extra slices are needed at each end of the volume (expanding the z dimension) due to the "long-object problem" [5]. Estimating correctly these slices outside the ROI is important as they may impact the estimation of voxels inside the ROI. In helical CT, these extra slices are only sparsely sampled by the projection views (see Fig. 1(a)). This sparse sampling can lead to very imbalanced subsets, particularly for large L, which can destabilize standard OS methods, degrading image quality.

The idea underlying regularized OS algorithms for CT is to use the gradient of a subset of the data fidelity term to approximate the gradient of the full data-fit term. Standard regularized OS algorithms simply scale the subset gradient by the constant L [3]. This works fine in 2D, but does not account for the sampling geometry outside ROI in helical CT, leading to degraded images particularly for large L. Section II-C proposes new scaling factors that stabilize the regularized OS algorithm for helical CT. The idea may be translated to other geometries with non-uniform geometric sampling. Like standard OS algorithms, the proposed approach is not guaranteed to converge (except for the one subset version).

OS algorithms can be modified so that they converge by introducing relaxation [6], reducing L, or by incremental optimization transfer [7]. The new scaling factors could be combined with such methods. Unfortunately, such methods converge slower than standard OS algorithms. Section III investigates practical methods for improving image quality of regularized OS algorithms without slowing initial convergence.

Results with real helical CT data illustrate that the proposed approach provides improved image quality and better convergence behavior than the ordinary OS algorithm in [3].

II. Theory

We reconstruct an image $x = (x_1, \ldots, x_N) \in \mathbb{R}^N$ from noisy measurement data $y \in \mathbb{R}^M$ by minimizing a penalized weighted least-squares cost function [1]:

$$\Psi(x) = Q(x) + \beta R(x) = \frac{1}{2}||y - Ax||_W^2 + \beta R(x)$$
$$= \sum_{i=1}^{M} q_i([Ax]_i) + \beta \sum_{k=1}^{K} \psi_k([Cx]_k), \quad (1)$$

where $A = \{a_{ij}\}$ is a projection matrix, $C = \{c_{kj}\}$ is a finite differencing matrix, the diagonal matrix $W = \mathsf{diag}\{w_i\}$ provides statistical weighting, and $q_i(t) = \frac{1}{2} w_i (t - y_i)^2$, each $\psi_k(t)$ is a potential function, and β is a regularization parameter.

A. Separable quadratic surrogate (SQS) algorithm

In this paper, we consider OS algorithms for minimizing the cost function (1) that are based on separable quadratic surrogate (SQS) methods [3] that update all voxels simultaneously:

$$x_j^{(n+1)} = x_j^{(n)} - \frac{1}{d_j} \left([A' W (Ax^{(n)} - y)]_j + \beta \frac{\partial}{\partial x_j} R(x^{(n)}) \right), \quad (2)$$

D. Kim and J. A. Fessler are with the Dept. of Electrical Engineering and Computer Science, University of Michigan, Ann Arbor, MI 48109 USA (e-mail:kimdongh@umich.edu, fessler@umich.edu).

D. Pal and J.-B. Thibault are with GE Healthcare, Waukesha, WI 53188 USA (e-mail:debashish.pal@ge.com, jean-baptiste.thibault@med.ge.com).

Supported in part by GE Healthcare and NIH grant R01-HL-098686.

[1]Regularized OS algorithms with large L will have increased compute time per iteration due to repeated computation of the regularizer gradient, but this problem has been reduced in [4].

where we use a precomputed denominator d_j [3]. The denominator $d_j = d_j^Q + \beta d_j^R$ consists of $d_j^Q = [A'WA1]_j$ for the data-fit term and $d_j^R = [|C|'\Lambda|C|1]_j$ for the regularizer using maximum penalty curvature in [3], where $|C| = \{|c_{kj}|\}$ and $\Lambda = \text{diag}\left\{\max_t \ddot{\psi}_k(t)\right\}$. This paper focuses on OS-SQS algorithms, but the proposed ideas are applicable to other OS algorithms.

B. Ordered subsets (OS) algorithm

An OS algorithm for accelerating the SQS update (2) has the following lth sub-iteration at the nth iteration:

$$x_j^{(n+\frac{l+1}{L})} = x_j^{(n+\frac{l}{L})} - \frac{1}{d_j}\left(\hat{\gamma}_j^{(n+\frac{l}{L})}[A_l'W_l(A_l x^{(n+\frac{l}{L})} - y_l)]_j + \beta\frac{\partial}{\partial x_j}R(x^{(n+\frac{l}{L})})\right), \quad (3)$$

where l is the subset index. We count one iteration when all subsets are used once.

The update (3) would accelerate the SQS algorithm by exactly L if the scaling factor $\hat{\gamma}_j^{(n+\frac{l}{L})}$ satisfied the condition:

$$\hat{\gamma}_j^{(n+\frac{l}{L})} = \frac{[A'W(Ax^{(n+\frac{l}{L})} - y)]_j}{[A_l'W_l(A_l x^{(n+\frac{l}{L})} - y_l)]_j}. \quad (4)$$

This factor would be expensive to compute, so the conventional OS approach is to simply use the constant $\gamma = L$. This "approximation" often works well in the early iterations when the subsets are suitably "balanced," but in general the errors caused by the differences between $\hat{\gamma}_j^{(n+\frac{l}{L})}$ and γ cause OS methods to approach a limit-cycle that loops around the optimum of the objective function (1) [6], [7]. The next section describes a new approximation to the scaling factor $\hat{\gamma}_j^{(n+\frac{l}{L})}$ in (4) that stabilizes OS for helical CT.

C. OS algorithm with proposed scaling factors

The constant scaling factor $\gamma = L$ used in the ordinary regularized OS algorithm is reasonable when all the voxels are sampled uniformly by the projection views in all the subsets. But in geometries like helical CT, the voxels are non-uniformly sampled. In particular, voxels outside the ROI are sampled by fewer projection views than voxels within the ROI (see Fig. 1(a)). We propose to use a voxel-based scaling factor γ_j that considers the sampling rather than a constant factor γ. After investigating several candidates, we focused on the following scaling factor:

$$\gamma_j = \sum_{l=1}^{L} I_{\{[A_l'W_lA_l1]_j > 0\}}, \quad (5)$$

where $I_{\{B\}} = 1$ if B is true or 0 otherwise. As expected, $\gamma_j < L$ for voxels outside the ROI and $\gamma_j = L$ for voxels within the ROI.

Fig. 1(b) shows that the OS algorithm using the proposed scaling factors (5) provides better image quality than the ordinary OS approach which does not converge outside the ROI. The instability seen with the ordinary OS approach may also degrade image quality within the ROI as seen by the noise standard deviations in Fig. 1(b). Fig. 2 further shows that the ordinary OS algorithm within ROI is unstabilized due to the instability outside ROI, whereas the proposed OS algorithm being robust.

We precompute (5) and the data-fit denominator $d_j^Q \triangleq [A'WA1]_j = \sum_{l=1}^{L}[A_l'W_lA_l1]_j$ simultaneously to minimize the overhead of computing (5). We store (5) as a short integer for each voxel outside the ROI only, so it does not require significant memory.

III. Further refinements of OS algorithm

Although the new scaling factors (5) stabilize OS and improve image quality, the final image quality still is worse than a convergent algorithm (see Fig. 1(b)) because any OS method with constant scaling factors will not converge. This section discusses some practical methods that can improve image quality while maintaining reasonably fast convergence rates. These approaches help the OS algorithm come closer to

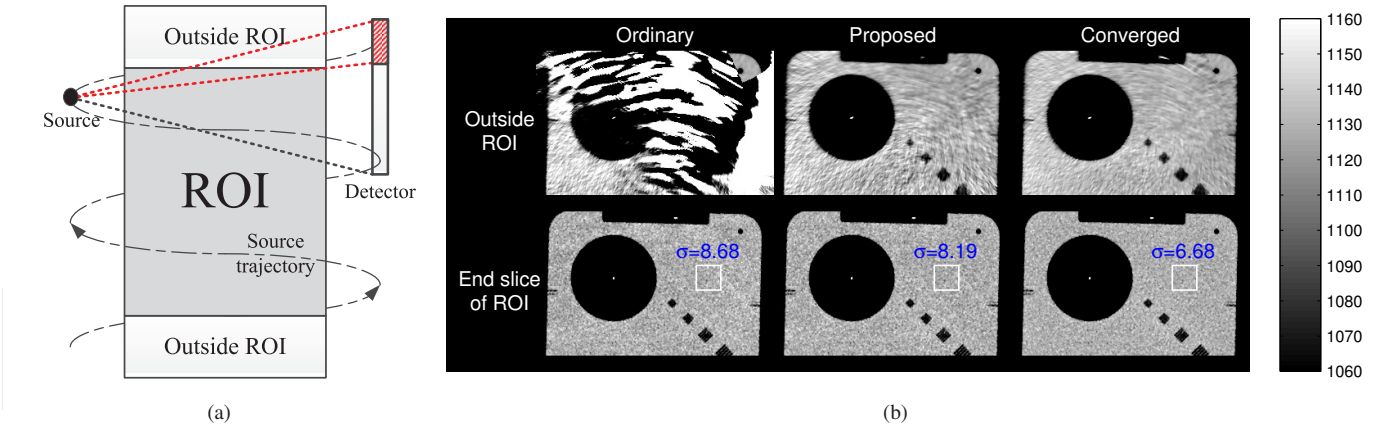

Fig. 1. Helical geometry and reconstructed images in the geometry: (a) Diagram of helical geometry. A (red) dashed region indicates the detector which acquires measurement data contributed by both voxels in ROI and voxels outside ROI. (b) Effect of gradient scaling in regularized OS-SQS algorithm with GE performance phantom (GEPP) in helical geometry: Each image is reconstructed after running 30 iterations of OS algorithm with 328 subsets, using ordinary and proposed scaling approaches. Standard deviation σ of a uniform region (in white box) is computed for comparison. (Several iterations of a convergent algorithm as a reference)

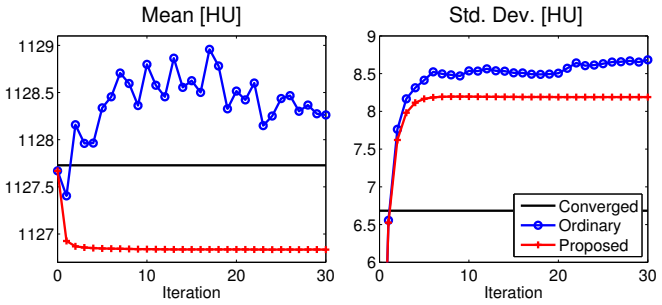

Fig. 2. Mean and standard deviation within an uniform region of end slice of ROI (See Fig. 1(b)) vs. iteration, showing the instability of ordinary OS approach compared with the proposed OS approach.

the converged image, reducing the undesirable noise in images reconstructed using OS algorithms with large L.

We investigated these methods using helical CT scans of the GE performance phantom (GEPP), shown in Fig. 4. We used mean and standard deviation of an uniform region to measure noise, full width at half maximum (FWHM) of a tungsten wire to measure resolution, and a root mean square difference (RMSD) between the OS image and a converged reference image.

A. Transition to small number of subsets

OS algorithm with large L is preferred for faster convergence, but it approaches a limit cycle leading to noisier images than to a converged solution. Using fewer subsets leads to images closer to the solution but slower convergence. A practical solution is to have fast initial convergence with many subsets and subsequently switch to fewer subsets to achieve a desirable final image. SQS converges slower for high spatial frequencies [8], and Table. I shows that an impulsive wire converges slowly for fewer subsets. Thus, the transition point must be chosen carefully to achieve fast convergence and desirable image quality. We found that 20 iterations with 328 subsets followed by 10 iterations with 82 subsets provided a reasonable balance between resolution and noise.

Because (5) depends on L, the transitioning approach requires computing another set of γ_j factors for the smaller number of subsets. For the choice of switching from 328 to 82 subsets, we can precompute both $\gamma_{j,328}$ and $\gamma_{j,82}$ efficiently along with the precomputed data-fit denominator using the following equations:

$$\gamma_{j,328} = \sum_{p=1}^{82} \sum_{l=4p-3}^{4p} I_{\{[A_l' W_l A_l 1]_j > 0\}}$$
$$\gamma_{j,82} = \sum_{p=1}^{82} I_{\{\sum_{l=4p-3}^{4p} I_{\{[A_l' W_l A_l 1]_j > 0\}} > 0\}}. \quad (6)$$

Because 328 is divisible by 82, each group of 4 consecutive subsets out of 328 subsets matches one of the 82 subsets.

B. Averaging sub-iterations at termination

To ensure convergence, [7] proposed to average previous sub-iterations, but the greatly increased memory space required has prevented its application in 3D X-ray CT. As a practical alternative, we investigated an approach where the final image is formed by averaging all of the sub-iterations of the final iteration of the OS algorithm (after it approaches its

	Smoothed	Number of subsets			Suggested approaches			Conv.
	FBP	82	246	328	Trans.	Aver.	Tr.&Av.	
Mean [HU]	1126.2	1126.2	1125.4	1125.2	1126.2	1126.3	1126.4	1126.4
Std. Dev. [HU]	2.22	6.91	7.58	8.02	7.01	7.38	6.97	6.81
FWHM [mm]	1.36	0.72	0.61	0.60	0.61	0.60	0.61	0.59
RMSD [HU]	18.48	2.20	2.99	4.03	1.58	2.31	1.36	·

TABLE I
NOISE, RESOLUTION AND RMSD BEHAVIOR OF OS ALGORITHM FOR EACH APPROACHES AFTER 30 ITERATIONS, COMPARED WITH SMOOTHED FBP AND CONVERGED IMAGE.

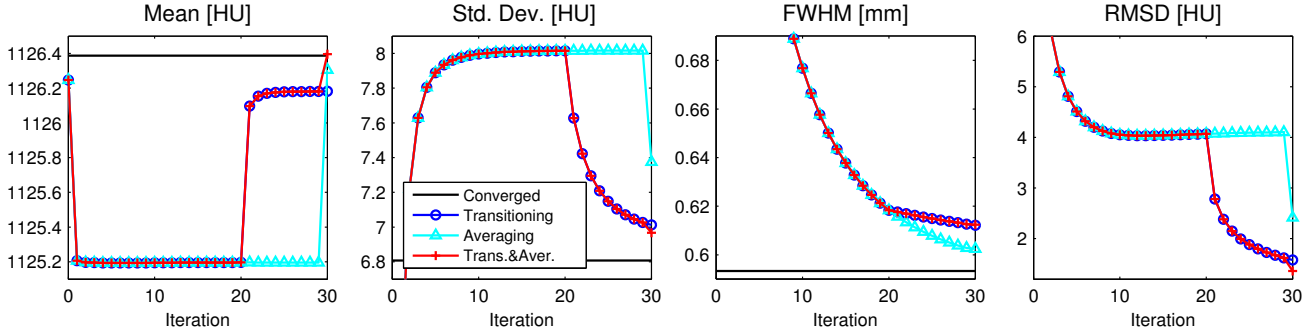

Fig. 3. Noise (mean and std. dev.), resolution (FWHM) and RMSD of OS-SQS with three suggested approaches vs. iteration. Three methods improved image quality of OS algorithm without slowing down the fast convergence rate.

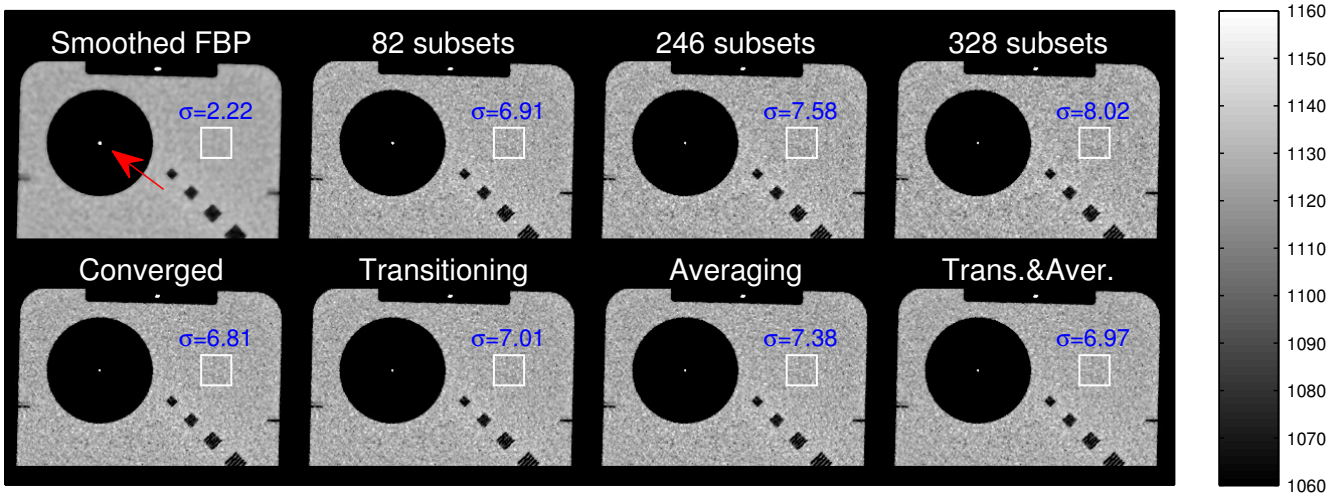

Fig. 4. Smoothed FBP, converged image and OS-SQS reconstructed images after 30 iterations. We used the uniform region within the white box to measure the noise level and σ indicates the standard deviation of the uniform region. We computed the FWHM of a wire (red arrow) to measure the resolution.

limit cycle). We ran 30 iterations of 328 subsets and averaged the 328 sub-iterations of the final iteration. A memory-efficient implementation of this approach uses a recursive in-place calculation:

$$\bar{x}^{(\frac{l+1}{L})} = \frac{l}{l+1}\bar{x}^{(\frac{l}{L})} + \frac{1}{l+1}x^{(\frac{l+1}{L})}, \qquad (7)$$

where $\bar{x}^{(1)}$ is the final averaged image.

We also investigated the combination of transitioning and averaging approaches. We averaged the 82 sub-iterations of the final iteration, after running 20 iteration of 328 subsets and 10 iterations of 82 subsets.

C. Results

We examined the effects of the three suggested methods applied to OS algorithms with 328 subsets. Fig. 4 shows the smoothed filtered back-projection (FBP) image and converged reference image, where we use the smoothed FBP image as the initial condition for the iterative algorithms. Table. I, Fig. 3 and Fig. 4 show that all methods help improve overall image quality, whereas the resolution slightly degraded compared with solely using 328 subsets. Both transitioning and averaging greatly helped reducing the noise in the images.

Transitioning to small number of subsets decreased the noise level but using fewer subsets impacted somewhat the convergence of high-frequency structures in the image. In contrast, averaging sub-iterations over the last iteration maintained the resolution level but the noise did not decrease as much as the transitioning approach. A combination of both the approaches compensates for the drawbacks of each and is a feasible solution.

IV. Discussion

We proposed a new scaling approach (5) for a regularized OS algorithm that provides an efficient solution for non-uniformity in the sampling geometry such as in helical CT. This approach reverts to the standard regularized OS algorithm in the middle of the ROI where the voxels are all well sampled, but stabilizes the images in the slices outside of the ROI where the standard constant scaling factor leads to over-correction, particularly when using many subsets. In addition, we investigated some practical approaches for improving the image quality after OS approaches a limit cycle, namely, transitioning to fewer subsets and averaging the sub-iterations of the final iteration. Preliminary results suggest that these methods can improve the overall image quality of OS algorithms when using numerous subsets without unduly affecting the convergence rate. Future work includes seeking a theoretical justification for the proposed scaling factors (5).

References

[1] J-B. Thibault, K. Sauer, C. Bouman, and J. Hsieh, "A three-dimensional statistical approach to improved image quality for multi-slice helical CT," *Med. Phys.*, vol. 34, no. 11, pp. 4526–44, Nov. 2007.

[2] H. M. Hudson and R. S. Larkin, "Accelerated image reconstruction using ordered subsets of projection data," *IEEE Trans. Med. Imag.*, vol. 13, no. 4, pp. 601–9, Dec. 1994.

[3] H. Erdoğan and J. A. Fessler, "Ordered subsets algorithms for transmission tomography," *Phys. Med. Biol.*, vol. 44, no. 11, pp. 2835–51, Nov. 1999.

[4] J. H. Cho and J. A. Fessler, "Accelerating ordered-subsets image reconstruction for X-ray CT using double surrogates," in *Proc. SPIE 8313, Medical Imaging 2012: Phys. Med. Im.*, 2012, To appear at 8313-69.

[5] M. Defrise, F. Noo, and H. Kudo, "A solution to the long-object problem in helical cone-beam tomography," *Phys. Med. Biol.*, vol. 45, no. 3, pp. 623–43, Mar. 2000.

[6] S. Ahn and J. A. Fessler, "Globally convergent image reconstruction for emission tomography using relaxed ordered subsets algorithms," *IEEE Trans. Med. Imag.*, vol. 22, no. 5, pp. 613–26, May 2003.

[7] S. Ahn, J. A. Fessler, D. Blatt, and A. O. Hero, "Convergent incremental optimization transfer algorithms: Application to tomography," *IEEE Trans. Med. Imag.*, vol. 25, no. 3, pp. 283–96, Mar. 2006.

[8] K. Sauer and C. Bouman, "A local update strategy for iterative reconstruction from projections," *IEEE Trans. Sig. Proc.*, vol. 41, no. 2, pp. 534–48, Feb. 1993.